

Original Research Article

Clinical rationale for *in vivo* portal dosimetry in magnetic resonance guided online adaptive radiotherapy

Begoña Vivas Maiques^{1,*}, Igor Olaciregui Ruiz¹, Tomas Janssen, Anton Mans

Department of Radiation Oncology, The Netherlands Cancer Institute, Antoni van Leeuwenhoek, Plesmanlaan 121, 1066 CX Amsterdam, The Netherlands



ARTICLE INFO

Keywords:

In vivo dosimetry
EPID
MR-Linac
Unity
Online adaptation
Verification

ABSTRACT

Background and purpose: In magnetic resonance guided online adaptive radiotherapy, the patient model used for plan adaptation and dose calculation is created online under stringent time constraints. This study investigated the ability of *in vivo* portal dosimetry to detect deviations between the online patient model used for plan adaptation and the actual anatomy of the patient during delivery.

Materials and methods: Portal images acquired during treatment were used to reconstruct the delivered dose corresponding to online adapted plans of 42 prostate and 20 rectal cancer patients. The reconstructed dose distributions were compared with the dose distributions calculated online by the treatment planning system by γ -analysis and by the difference in median dose to the high-dose volume.

Results: Out of 245 prostate and 145 rectal cancer adapted plans, deviations were detected in 5 prostate and in 17 rectal adapted plans corresponding to 3 prostate and 6 rectal patients, respectively. For all but one of the alerts, deviations were explained due to discrepancies observed between the patient model used for plan adaptation and online magnetic resonance images. A single workflow incident in which the supporting arm of the anterior receive coil was accidentally moved in the treatment field was also detected.

Conclusion: There is need for independent end-to-end checks in magnetic resonance guided online adaptive workflows including the verification of the online patient model. *In vivo* portal dosimetry can be used for such purpose as it can detect both patient related deviations and workflow incidents.

1. Introduction

Magnetic resonance (MR) guided radiotherapy allows for online adaptive workflows [1–3]. In each treatment fraction, online pre-treatment MR images are used as input to plan to the daily patient anatomy either by adapting the contours or by shifting the patient position. Online adaptive strategies need to be executed under stringent time constraints as online patient model creation, plan adaptation and dose calculation must be performed while the patient is on the treatment couch [4–8]. The majority of these are semi-automated steps requiring human intervention to validate and complete the process. In the patient model creation step, online human contour reviewing and/or editing is required. In a recent study, wrong re-contouring by the physician of the day and considerable errors in the assignment of the electron density for online dose calculation were among the most critical risks detected in magnetic resonance guided online adaptive radiotherapy [9]. Therefore, as a degree of error is inevitable in human tasks, one would wish to have

patient specific quality assurance (PSQA) tools in place that could detect discrepancies between the patient model that was accepted and used for plan adaptation and the actual position and anatomy of the patient during delivery.

Dosimetric PSQA is generally performed offline with MR-compatible detector devices capable of reconstructing a portion or the whole 3D dose distribution within a phantom [10–12]. The assessment is made by comparing the measured dose distribution to the planned dose distribution recalculated on the phantom geometry. These solutions are time-consuming, so checks are usually performed before treatment starts for the reference plan and, if time and resources allow, retrospectively, for (a subset of) the online delivered plans. Besides, they are not directly applicable for online adaptive workflows as they can detect transfer, machine or treatment planning system (TPS) errors but they don't verify the actual dose delivered to the patient.

Deep learning-based synthetic-CT images generated from MRI data [13–16] could be used in combination with independent dose

* Corresponding author.

E-mail address: b.vivas@nki.nl (B. Vivas Maiques).

¹ Begoña Vivas-Maiques and Igor Olaciregui-Ruiz share first authorship.

<https://doi.org/10.1016/j.phro.2022.06.005>

Received 22 December 2021; Received in revised form 7 June 2022; Accepted 8 June 2022

Available online 11 June 2022

2405-6316/© 2022 The Author(s). Published by Elsevier B.V. on behalf of European Society of Radiotherapy & Oncology. This is an open access article under the CC BY-NC-ND license (<http://creativecommons.org/licenses/by-nc-nd/4.0/>).

calculation algorithms for online ‘pre-treatment’ dosimetric verification of the adapted plans. Linac treatment log files, also combined with independent dose calculation algorithms and intrafraction MR imaging, have been used to estimate the daily delivered dose in prostate cancer treatments [17,18]. In this approach, each log entry is interpreted as a fluence package delivered to the specific patient anatomy at the time of delivery and the total delivered dose is estimated as the sum of these partial dose calculations. Dynamic patient models must be automatically created for each partial dose calculation. Despite the strong application demand, none of these methodologies are widely adopted yet.

An alternative approach to verify the daily delivered dose, and hence the patient model utilized for online plan adaptation, would be the use of *in vivo* portal dosimetry. Portal images contain information about the actual patient anatomy during treatment. The dose is estimated by back-projecting the portal image data to the patient model that was used for online plan adaptation. In cases where the patient model does not correctly account for the patient anatomy during delivery, the reconstructed dose does not estimate the actual delivered dose but can be used to determine deviations from the planned delivery. Previous work demonstrated the feasibility of *in vivo* portal dosimetry in MR-guided adaptive workflows [19,20]. This study investigated the ability of *in vivo* portal dosimetry to detect deviations between the online patient model used for plan adaptation and the patient anatomy during delivery.

2. Methods and materials

2.1. Equipment

The Unity MR-Linac is a combination of a 7 MV flattening filter free (FFF) beam linac (Elekta AB, Stockholm, Sweden) and an integrated 1.5 T MRI scanner (Phillips Medical Systems, Best, The Netherlands) [2,21]. The Unity MR-Linac is equipped with an electronic portal image device (EPID) which is mounted on the rotating gantry opposite to the accelerator head [22]. Although originally designed for position verification and other QA or calibration purposes, the detector has proven to be suitable for *in vivo* dosimetry applications [23]. EPID images were acquired during patient treatment with Elekta’s MV imaging controller (MVIC) acquisition software. Treatment plans were generated using Monaco 5.4 (Elekta AB, Stockholm, Sweden) treatment planning system (TPS). Plans for both rectal and prostate cancer were generated using 9-beam IMRT techniques similar to the ones described in [24]. The fractionation schemes were 5x5Gy or 25x2Gy for rectal cancer and 5x7Gy with a focused boost 5x10Gy or 20x3Gy for prostate cancer. All plans were optimized following the ‘Optimize Weights and Shapes from fluence’ method [3]. Online plan adaptation on the Unity system can be performed through two workflows: adapt to position (ATP) and adapt to shape (ATS) [3]. In the ATP workflow, the online patient model is obtained by a rigid registration of the reference planning CT to the online MRI images. Plan re-optimization is performed on the shifted reference CT and contours. This is only a first order correction as the shift of the plan cannot correct for (1) target rotations, (2) changes in target volume and shape and (3) changes in the geometric relationship between target and surrounding structures [25]. In the ATS workflow, the online patient model is obtained by propagation of the reference contours to the online MRI. The adapted contours are assigned a bulk electron density based on the average value of the corresponding contour in the reference CT. The online plan is then re-optimized on the online planning MRI with adjusted contours.

2.2. EPID dosimetry

The back-projection algorithm uses EPID images acquired during delivery to reconstruct 3D dose distributions within the same online patient model that was used for online plan adaptation. The online patient model was used to estimate the primary portal dose transmission, which together with the measured primary portal dose distribution were

the main inputs to the algorithm. The parameters of the algorithm are determined during the commissioning process using absolute dose measurements and EPID measurements made behind water-equivalent phantoms. Without corrections for tissue inhomogeneities, the reconstructed dose distributions are accurate only for reconstructions in nearly water-equivalent material as typically is the case in treatment disease sites such as prostate and rectal cancer. In the presence of significant tissue inhomogeneities, the *in aqua* approach was used [26].

2.3. Dosimetric evaluation

The comparison was performed by γ -analysis using the same parameters as in conventional linacs (3% global/3mm/50% threshold) [27]. The choice for a threshold value of 50% of the maximum planned dose for γ -statistics is arbitrary, but a threshold is necessary to separate low and high dose areas. Including the lower-dose regions would lower the average and conceal differences. As dose reconstruction is accurate for the parts of beam that reach the detector through the central region of the cryostat free of gradient coils and shimming hardware, the comparison was restricted to the volume where the EPID receives ‘un-attenuated’ signal [19]. The tolerance limits used were 0.7, 2.0 for γ -mean and γ -max, respectively. For γ -pass rate, an 85% limit was used for prostate cancer and a 75% limit was used for rectal cancer. A lower threshold value was selected for rectal cancer due to the extra uncertainties in dose reconstruction for rectum fields, usually with sizeable parts reaching the detector outside the central un-attenuated region [20,28]. To report on dose differences, deviations in median dose to the high-dose volume (ΔHDV_{D50}) were also evaluated. HDV was defined as the volume surrounded by the surface encompassing 90% of the maximum planned dose. The tolerance limit was 5%. The tolerance limit values were chosen for an optimal balance between resources and detection of patient model errors at end of the RT chain. With these tolerance limit values, the system is not likely to detect plan-specific machine deviations, as these are usually small. Certainly, the system should be able to detect more serious machine errors [29] but such failure modes are expected to have very low occurrence, particularly if comprehensive machine QA tests are performed on a weekly basis [9,30].

Online adapted plans with all indicators within tolerance were automatically approved, alerts were raised otherwise. As the framework was configured to run at the end of the day, alert inspection took place usually on the following morning. The inspection work involved consistency checks, examination of the portal images and inspection of the available online MRI images. For all the detected deviations, *in air* EPID measurements (without the patient in the beam) were performed to reconstruct virtual patient dose distributions. Virtual and *in vivo* patient dose distributions are similarly affected by machine, planning and EPID commissioning model errors. Differences between virtual and *in vivo* dose verification results usually indicate the presence of patient-related deviations [31]. If deviations still remain unexplained, a measurement with an MR-compatible detector device could be performed.

2.4. Patient data

EPID data corresponding to 42 prostate and 20 rectal cancer patients treated in the period from January until August 2021 were included in this study. The *in aqua* approach was used in one prostate treatment for which large air pockets were delineated in the reference planning CT. A total number of 245 prostate and 145 rectal cancer adapted plans were verified by comparing EPID-reconstructed dose distributions with dose distributions calculated online by the TPS [20]. The patients were included in three studies, approved by the medical ethics committee (NCT04045717, NCT02945566 and NCT04075305) of the Netherlands Cancer Institute and written informed consent was obtained.

3. Results

In the *in vivo* verification of 245 prostate and 145 rectal cancer adapted plans, the γ -pass rate median (interquartile range) values were 98.9% (4.5%) and 90.1% (13%) for prostate and rectal cancer treatments, respectively. The $\Delta\text{HDV}_{\text{D50}}$ average (1SD) values were -0.8 (2.1) and -1.3 (2.4), respectively. Fig. 1 displays histograms of the *in vivo* EPID dosimetry results. Deviations were detected in 5 prostate and in 17 rectal plans corresponding to 3 prostate and 6 rectal patients, respectively. Table 1 summarizes information of the detected deviations. EPID virtual patient dose reconstructions for the alerted adapted plans agreed well with online TPS calculations. This suggests that the root cause of the detected *in vivo* deviations were patient model related. No measurements with MR-compatible detector devices were performed.

The alert for patient #1 was raised for the 11th ATP adaptation of a 20x3Gy prostate cancer treatment. Under-dosages of $\sim 15\%$ were reported for a large volume. Inspection of the EPID images revealed the presence of one of the supporting arms of the coil holder in the EPID transit images, see Fig. 2. The beams were accidentally attenuated by the supporting arm of the coil before reaching the EPID.

The alerts for patient #2 were raised for 3 out of 5 fractions in a 5x7Gy with a focused boost of 5x10Gy prostate cancer treatment. Fig. 3 displays registration results for one alerted plan. Online MR images revealed that a significant amount of patient body volume was left outside the rigidly shifted reference body contour that was used for online patient model creation.

The alerts for patients #3, #4, #7 and #8 revealed tissue density changes that were not considered during online plan adaptation. For

in vivo EPID dosimetry results

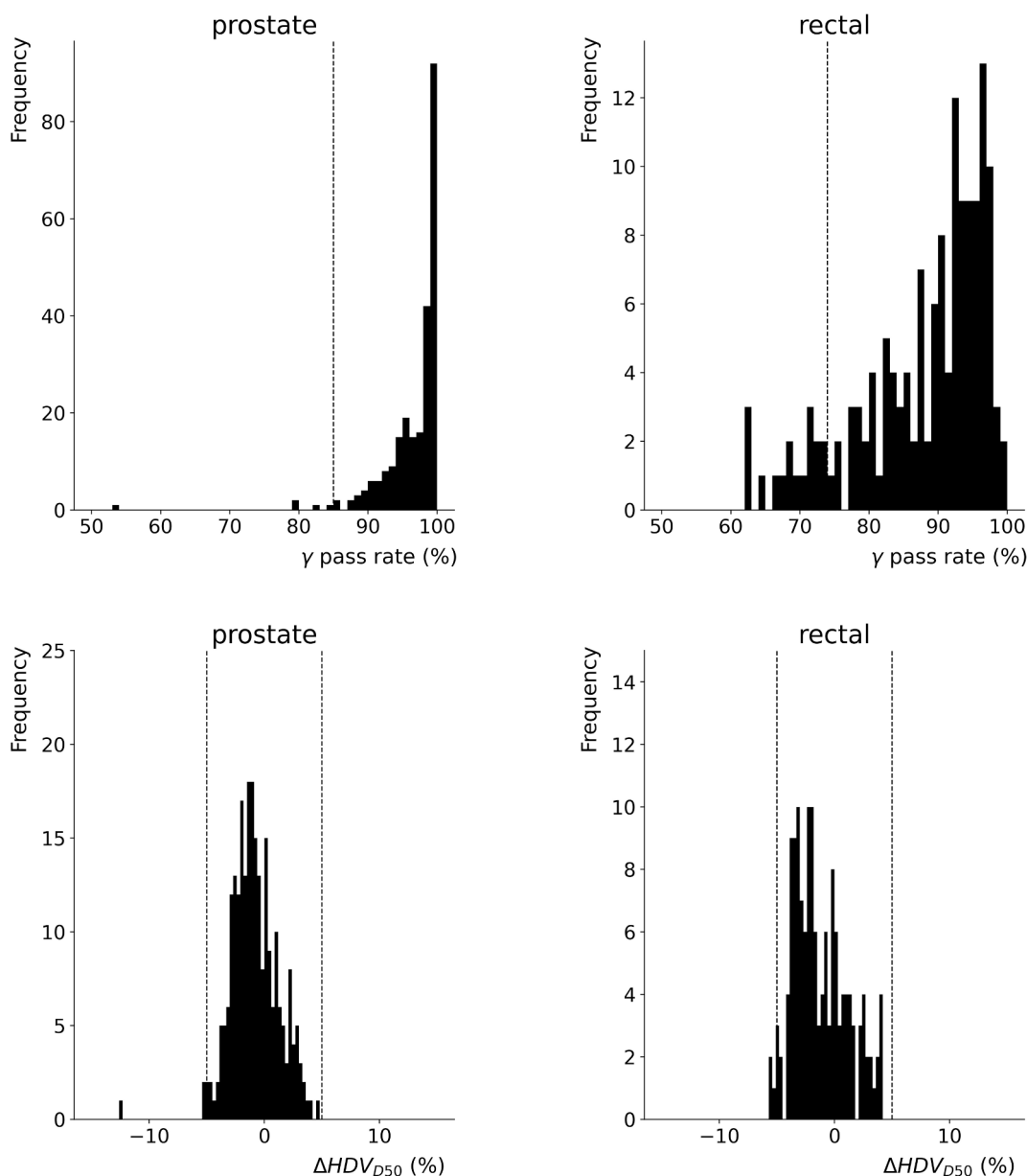


Fig. 1. Histograms of γ -pass rate and $\Delta\text{HDV}_{\text{D50}}$ EPID dosimetry results corresponding to the *in vivo* verification of 245 prostate and 145 rectal cancer adapted plans. The dotted black vertical lines represent the tolerance limit values used for error deviation detection.

Table 1

Summary information of the 3 prostate and 6 rectal cancer patients reporting at least one fraction out of tolerance. The table presents the number of alerted and non-alerted fractions with the indicator that raised the alert. Average results are displayed for alerted *in vivo* fractions, non-alerted *in vivo* fractions and virtual dose reconstructions separately. As specified in the indicator column, results are presented as γ -pass rate values (%) except for case #2 (% Δ HDV_{D50}).

Tumor site	Patient	# alerts / non alerts	Indicator	Average result		
				<i>In vivo</i> alerts	<i>In vivo</i> non alerts	Virtual reconstructions
prostate	#1	1 / 19	γ pass-rate (%)	54	94	91
	#2	3 / 2	Δ HDV _{D50} (%)	-5.1	-4.1	-1.8
	#3	1 / 19	γ pass-rate (%)	80	92	98
rectal	#4	3 / 2	γ pass-rate (%)	72	83	94
	#5	5 / 20	γ pass-rate (%)	62	87	97
	#6	2 / 3	γ pass-rate (%)	70	89	96
	#7	1 / 4	γ pass-rate (%)	72	94	90
	#8	1 / 4	γ pass-rate (%)	62	85	98
	#9	5 / 0	γ pass-rate (%)	73	x	99

Patient #1 : Workflow incident

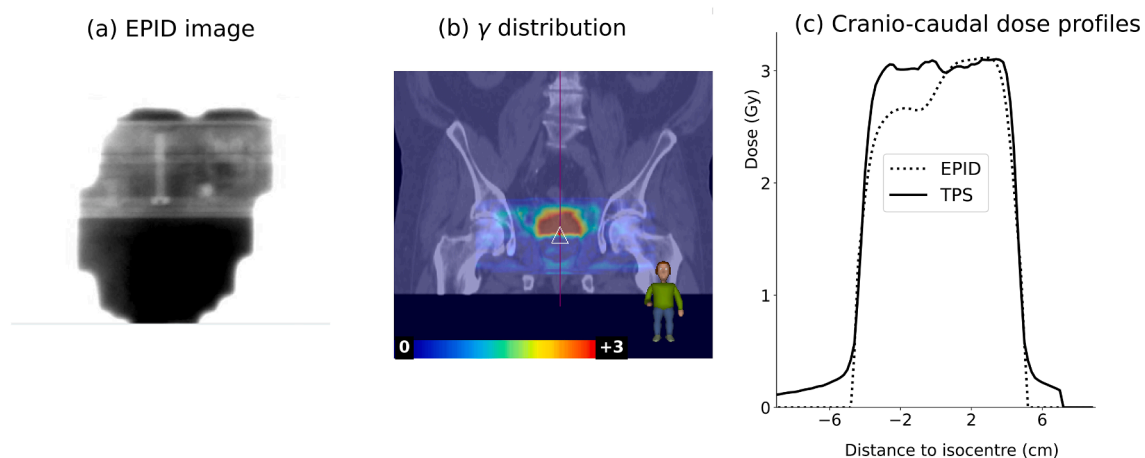


Fig. 2. a) EPID image recorded during the delivery of a 20x3Gy prostate cancer treatment showing the accidental presence of one of the supporting arms of the anterior RF coil in the beam, b) coronal slice of the 3D γ distribution corresponding to the comparison between the EPID reconstructed and the TPS calculated dose distributions, c) dose profiles along the cranio-caudal direction through the isocentre. The beams were attenuated by the anterior RF coil that had been accidentally pushed towards the feet of the patient before the start of irradiation. The center of the white triangle in (b) corresponds to the isocentre.

patient #4, alerts were raised for 3 out of 5 ATS adaptations in a 5x5Gy rectal cancer treatment. Inspection of online pre-treatment MR images for the three alerted fractions revealed an empty bladder in a patient that followed a full bladder preparation protocol, see Fig. 4. In patients #7 and #8, air pockets visible on online pre-treatment MR images were not delineated online in the ATS workflow and hence were not considered (missing) for dose calculation. For patient #3, the situation was opposite. Air pockets delineated in the reference CT that were not visible on online pre-treatment MR images were retained for dose calculation in a prostate ATP adaptation.

The alerts for patients #5 and #6 exposed patient anatomy changes between the online pre-treatment MRI images used for online plan adaptation and extra online post-treatment MR images acquired shortly before the end of irradiation, see Fig. 5.

Alerts were raised for all fractions of patient #9. The average Δ HDV_{D50} deviation was +3.7%. Inspection of online pre-treatment MR images revealed that the external contour had not been propagated correctly, possibly due to an artifact on the MR image due to breathing motion.

4. Discussion

In this study, we have demonstrated how *in vivo* EPID dosimetry can

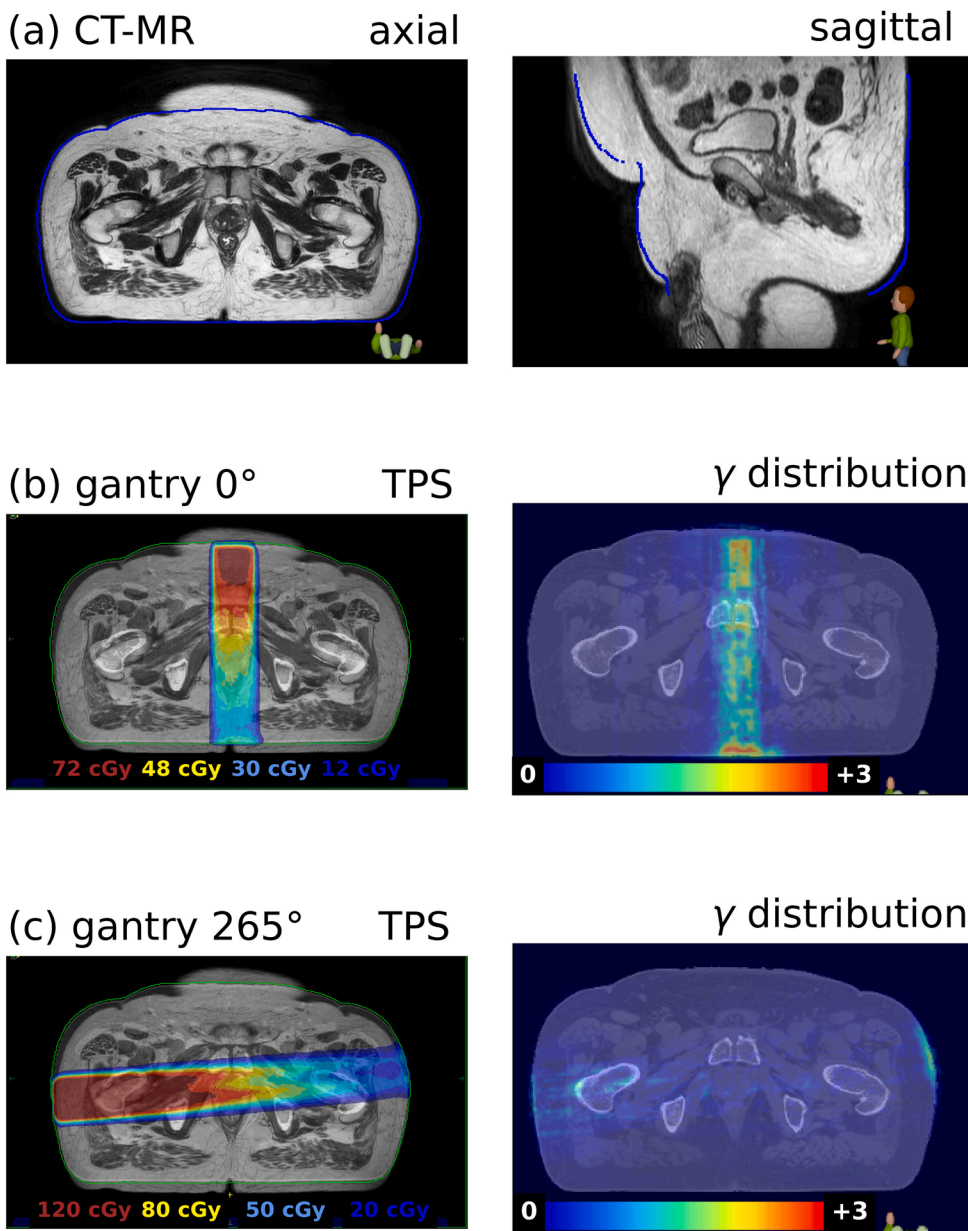
be used as an independent and automated end-to-end check in MR-guided online adaptive workflows, primarily concerning the correctness of the online patient model used for plan adaptation and dose calculation but also with regards to workflow incidents.

Regarding the incident for Patient #1, the Unity MR-Linac is equipped with a radiofrequency (RF) receive coil that allows for online MR guidance without having a significant impact on both treatment delivery and outer contour of the patient [32]. The posterior coil is positioned under the table. The anterior coil rests on a coil holder supported by two arms of high density material, which attach it to the patient support system. During treatment, its position is fixed with breaks, which are intentionally built as 'soft breaks' because of patient safety. It was concluded that the anterior coil had been accidentally pushed towards the feet of the patient before the start of irradiation. As this was a 20-fraction treatment and all other fractions were correctly delivered, no action was taken in this particular case. However, extra checks are currently being made in the treatment room to ensure the correct positioning of the coil and prevent potentially more hazardous errors such would be the case for single (or few fractionated) radiation treatments like stereotactic body radiation therapy treatments.

The alerts for patient #2 and #9 detected discrepancies in patient body contours. The alerts for patient #2 highlight the need to review (and possibly edit) the external body contour during registration. A

Patient #2 : Body contour changes

Fig. 3. Rigid registrations of the reference planning CT to online pre-treatment MR images (a), online TPS dose calculations and γ distributions for beams at gantry angles 0° (b) and 265° (c) for an alerted ATP adaptation of a 5x7Gy with a focused boost of 5x10Gy prostate cancer treatment. (a) displays a significant amount of patient body volume left outside the rigidly shifted reference body contour that was used for online dose calculations. The rigidly propagated external body contour is coloured in blue. EPID dosimetry detected under dosages for the beams traversing through the unaccounted patient thickness before reaching the detector, e.g beam at gantry angle 0° .



likely explanation for these alerts was that this patient used a pair of tight fitting trousers both during planning and during treatment, which were in a slightly different position around the waist each time. The under dosages to the tumour volume were estimated to be $\sim 2.5\%$ as half of the beams for which deviations were detected were posterior beams traversing the unaccounted patient thickness after reaching the patient. No clinical action was taken. For patient #9, the automatically adapted contours of the patient were somewhat larger than the actual contours visible in the MRI scan, which explained the overdose in the ΔHDV_{D50} deviation results. EPID re-calculations made with the original contour of the reference CT reported γ -pass rate and ΔHDV_{D50} values around 95% and 1.5%, which suggested that the reference external contours were a better representation of the patient body contour than the adapted contours. No clinical action was taken for this particular treatment but clinical protocols are being proposed to check for these artifacts during the propagation of external body contours in ATS

workflows.

Likewise, the alerts for patients #3, #4, #7 and #8 urge the review of existing contours together with their assigned densities. In the alerts for patient #4, the daily bladder contour was assigned a bulk electron density based on the average value of the (full) bladder contour in the reference CT. Since the electron density assigned to a full bladder is higher than the electron density assigned to the bowel (which is a mixture of air, faeces and tissue), the attenuation of the beams during delivery was less than what was expected and a higher signal reached the detector as result. Similarly, for patients #3, #7 and #8, the dosimetric effect of the missing/retained air pockets was detected by EPID dosimetry. The deviations detected for patients #5 and #6 were explained by air pockets visible only on post-treatment online MR images, proving that EPID dosimetry can provide additional assistance in the detection of intrafraction anatomy changes. Overall, deviations were detected only in a small percentage of treatment fractions (22 out 390

Patient #4 : Tissue density changes

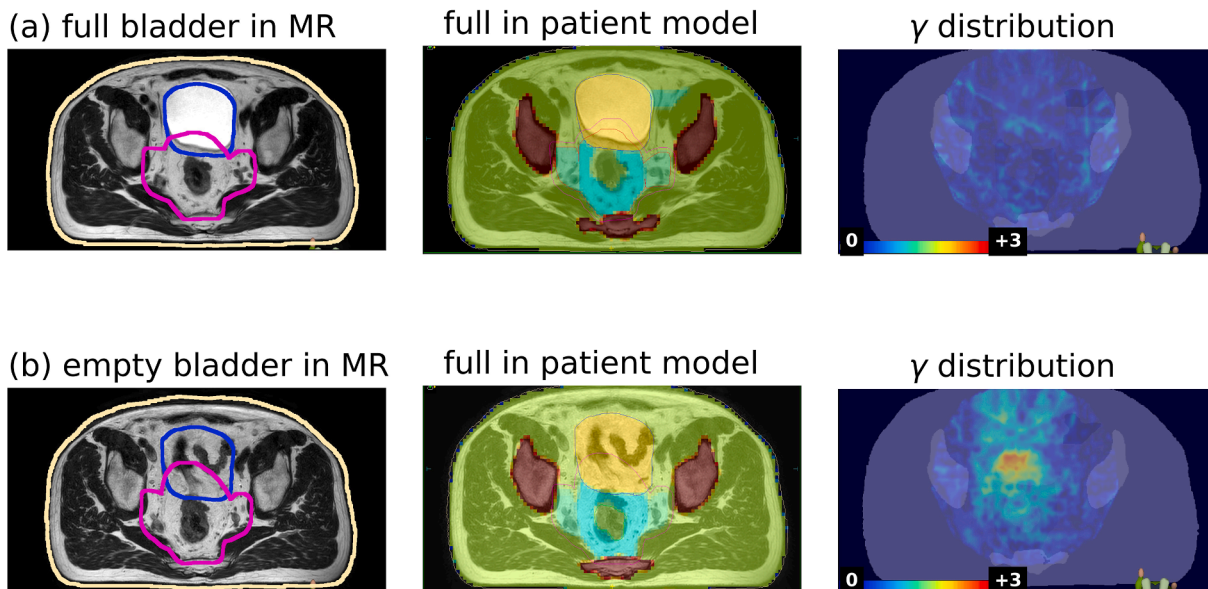


Fig. 4. Axial views of online pre-treatment MR images, online patient models used for plan re-adaptation and γ distributions for two ATS adaptations of a 5x5Gy rectal cancer treatment: a non-alerted fraction displaying a full bladder in MR images (a), and an alerted fraction displaying an empty bladder in MR images (b). Rectal cancer patients adhere to a drinking protocol aiming at a full bladder both during planning and during treatment. The dosimetric effect of retaining a full bladder in the patient model in (b) was detected by EPID dosimetry.

Patient #5: Pre- and post-irradiation changes

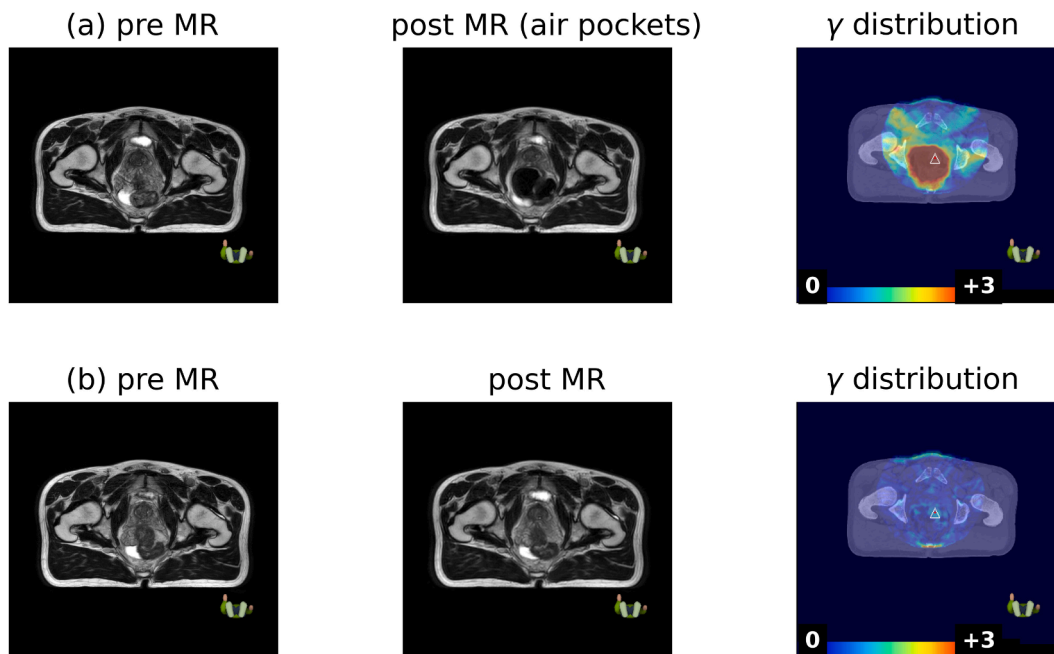


Fig. 5. Axial views of online pre- and post-treatment MR images and γ distributions for two consecutive ATS adaptations of a 25x2Gy rectal cancer treatment, alerted (a) and non-alerted (b), respectively. In (a) significant patient density changes (air pockets) were observed during the 15 min which elapsed during plan adaptation and the end of treatment. These changes were detected by EPID dosimetry.

adapted fractions), which reassures the validity of the ATP and ATS workflows.

Studies with alternative dosimetric methods, such as the use of linac treatment log files in combination with intrafraction MR imaging,

yielded deviations also in a small subset of fraction [17,18]. The ability of independent dose calculation and/or log files based methods to detect patient-related deviations will depend on how accurately the provided synthetic-CT image and/or dynamic patient models represent the actual

patient anatomy during delivery. In one of the methods, dynamic patient models were created by bulk density assignment of the corresponding cine-MR following the same method used during the initial planning [17]. In the other method, the dynamic patient models were not able to resolve rotations, deformations and density changes affecting the beam's attenuation [18]. Simpler non-dosimetric solutions have also been proposed to check irregularities during the plan adaptation and patient model creation processes including contour analysis, electron density map examinations, and fluence modulation complexity controls. In a recent study [33], irregularities were found in 9 out of 362 adapted fractions.

The main advantage of EPID dosimetry over other methods is that portal images contain direct information related to the absorbed dose in the patient and hence can catch freak incidents such as #1. The limitations of EPID dosimetry are the following: the simplicity of the reconstruction model, the limited 'attenuation-free' active area of the detector and the fact that detection is only possible after treatment. Therefore, the use of in portal dosimetry in combination with other PSQA methods could provide additional advantages. Independent dose calculations made with synthetic-CT images, for example, could help discriminate between false and true positives during the inspection work and to estimate the dosimetric impact of the deviations.

In conclusion, there is need for independent end-to-end checks in magnetic resonance guided online adaptive workflows including the verification of the online patient model. In vivo portal dosimetry can be used for such purpose as it can detect both patient related deviations and workflow incidents.

Declaration of Competing Interest

The Netherlands Cancer Institute is a member of the Elekta AB (Stockholm, Sweden) MR-Linac consortium. In addition, our department has a collaboration agreement with PTW (Freiburg, Germany) to jointly develop an EPID-based dosimetry solution for automated patient-specific quality assurance in radiotherapy.

References

- 1] Lagendijk JJW, Raaymakers BW, Van Den Berg CAT, Moerland MA, Philippens ME, Van Vulpen M. MR guidance in radiotherapy. *Phys Med Biol* 2014;59:R349–69. <https://doi.org/10.1088/0031-9155/59/21/R349>.
- 2] Raaymakers BW, Lagendijk JJW, Overweg J, Kok JGM, Raaijmakers AJE, Kerkhof EM, et al. Integrating a 1.5 T MRI scanner with a 6 MV accelerator: Proof of concept. *Phys Med Biol* 2009;54:N229. <https://doi.org/10.1088/0031-9155/54/12/N01>.
- 3] Winkel D, Bol GH, Kroon PS, van Asselen B, Hackett SS, Werensteijn-Honingh AM, et al. Adaptive radiotherapy: The Elekta Unity MR-linac concept. *Clin Transl Radiat Oncol* 2019;18:54–9. <https://doi.org/10.1016/j.ctro.2019.04.001>.
- 4] Christiansen RL, Dysager L, Bertelsen AS, Hansen O, Brink C, Bernchou U. Accuracy of automatic deformable structure propagation for high-field MRI guided prostate radiotherapy. *Radiat Oncol* 2020;15:1–11. <https://doi.org/10.1186/s13014-020-1482-y>.
- 5] K.A.J. Eppenhof M. Maspero M.H.F. Savenije J.C.J. de Boer van der Voort van Zyp JRN, Raaymakers BW, et al. Fast contour propagation for MR-guided prostate radiotherapy using convolutional neural networks *Med Phys* 47 2020 1238 1248 10.1002/mp.13994.
- 6] Künzel LA, Nachbar M, Hagmüller M, Gani C, Boeke S, Zips D, et al. First experience of autonomous, un-supervised treatment planning integrated in adaptive MR-guided radiotherapy and delivered to a patient with prostate cancer. *Radiother Oncol* 2021;159:197–201. <https://doi.org/10.1016/j.radonc.2021.03.032>.
- 7] Savenije MHF, Maspero M, Sikkes GG, Der Voort V, Van Zyp JRN, Alexis AN, et al. Clinical implementation of MRI-based organs-at-risk auto-segmentation with convolutional networks for prostate radiotherapy. *Radiat Oncol* 2020;15:1–12. <https://doi.org/10.1186/s13014-020-01528-0>.
- 8] Zhang Y, Paulson E, Lim S, Hall WA, Ahunbay E, Micekovic NJ, et al. A Patient-Specific Autosegmentation Strategy Using Multi-Input Deformable Image Registration for Magnetic Resonance Imaging-Guided Online Adaptive Radiation Therapy: A Feasibility Study. *Adv Radiat Oncol* 2020;5:1350–8. <https://doi.org/10.1016/j.adro.2020.04.027>.
- 9] Klüter S, Schrenk O, Renkamp CK, Gliessmann S, Kress M, Debus J, et al. A practical implementation of risk management for the clinical introduction of online adaptive Magnetic Resonance-guided radiotherapy. *Phys Imaging Radiat Oncol* 2021;17:53–7. <https://doi.org/10.1016/j.phro.2020.12.005>.
- 10] Houweling AC, De Vries JHW, Wolthaus J, Woodings S, Kok JGM, Van Asselen B, et al. Performance of a cylindrical diode array for use in a 1.5 T MR-linac. *Phys Med Biol* 2016;61:N80. <https://doi.org/10.1088/0031-9155/61/3/N80>.
- 11] De Vries JHW, Seravalli E, Houweling AC, Woodings SJ, Van Rooij R, Wolthaus JWH, et al. Characterization of a prototype MR-compatible Delta4 QA system in a 1.5 tesla MR-linac. *Phys Med Biol* 2018;63:02NT02. <https://doi.org/10.1088/1361-6560/aa9d26>.
- 12] Monnich D, Winter J, Nachbar M, Künzel L, Boeke S, Gani C, et al. Quality assurance of IMRT treatment plans for a 1.5 T MR-linac using a 2D ionization chamber array and a static solid phantom. *Phys Med Biol* 2020;65:16NT01. <https://doi.org/10.1088/1361-6560/aba5ec>.
- 13] Boulanger M, Nunes JC, Chourak H, Largent A, Tahri S, Acosta O, et al. Deep learning methods to generate synthetic CT from MRI in radiotherapy: A literature review. *Phys Med* 2021;89:265–81. <https://doi.org/10.1016/j.ejomp.2021.07.027>.
- 14] Tang B, Wu F, Fu Y, Wang X, Wang P, Orlandini LC, et al. Dosimetric evaluation of synthetic CT image generated using a neural network for MR-only brain radiotherapy. *J Appl Clin Med Phys* 2021;22:55–62. <https://doi.org/10.1002/acm2.13176>.
- 15] Kemppainen R, Suilamo S, Ranta I, Pesola M, Halkola A, Eufemio A, et al. Assessment of dosimetric and positioning accuracy of a magnetic resonance imaging-only solution for external beam radiotherapy of pelvic anatomy. *Phys Imaging Radiat Oncol* 2019;11:1–8. <https://doi.org/10.1016/j.phro.2019.06.001>.
- 16] Kazemifar S, McGuire S, Timmerman R, Wardak Z, Nguyen D, Park Y, et al. MRI-only brain radiotherapy: Assessing the dosimetric accuracy of synthetic CT images generated using a deep learning approach. *Radiother Oncol* 2019;136:56–63. <https://doi.org/10.1016/j.radonc.2019.03.026>.
- 17] C. Kontaxis D.M. de Muinck Keizer L.G.W. Kerkmeijer T. Willigenburg den Hartogh MD, van der Voort van Zyp JRN, et al. Delivered dose quantification in prostate radiotherapy using online 3D cine imaging and treatment log files on a combined 1.5T magnetic resonance imaging and linear accelerator system. *Phys Imaging Radiat Oncol* 15 2020 23 29 10.1016/j.phro.2020.06.005.
- 18] Menten MJ, Mohajer JK, Nilawar R, Bertholet J, Dunlop A, Pathmanathan AU, et al. Automatic reconstruction of the delivered dose of the day using MR-linac treatment log files and online MR imaging. *Radiother Oncol* 2020;145:88–94. <https://doi.org/10.1016/j.radonc.2019.12.010>.
- 19] Torres-Xirau I, Olaciregui-Ruiz I, Kaas J, Nowee ME, van der Heide UA, Mans A. 3D dosimetric verification of unity MR-linac treatments by portal dosimetry. *Radiother Oncol* 2020;146:161–6. <https://doi.org/10.1016/j.radonc.2020.02.010>.
- 20] Olaciregui-Ruiz I, Vivas-Maiques B, van der Velden S, Nowee ME, Mijnheer B, Mans A. Automatic dosimetric verification of online adapted plans on the Unity MR-Linac using 3D EPID dosimetry. *Radiother Oncol* 2021;157:241–6. <https://doi.org/10.1016/j.radonc.2021.01.037>.
- 21] Raaymakers BW, Jürgenliemk-Schulz IM, Bol GH, Glitzner M, Kotte ANTJ, et al. First patients treated with a 1.5 T MRI-Linac: Clinical proof of concept of a high-precision, high-field MRI guided radiotherapy treatment. *Phys Med Biol* 2017;62:L41–50. <https://doi.org/10.1088/1361-6560/aa9517>.
- 22] Raaymakers BW, De Boer JCJ, Knox C, Crijs SPM, Smit K, Stam MK, et al. Integrated megavoltage portal imaging with a 1.5 T MRI linac. *Phys Med Biol* 2011;56:N207. <https://doi.org/10.1088/0031-9155/56/19/N01>.
- 23] Torres-Xirau I, Olaciregui-Ruiz I, Baldivinsson G, Mijnheer BJ, Van Der Heide UA, Mans A. Characterization of the a-Si EPID in the unity MR-linac for dosimetric applications. *Phys Med Biol* 2018;63:025006. <https://doi.org/10.1088/1361-6560/aa9dbf>.
- 24] van de Schoot AJAJ, van den Wollenberg W, Carbaat C, de Ruitter P, Nowee ME, Pos F, et al. Evaluation of plan quality in radiotherapy planning with an MR-linac. *Phys Imaging Radiat Oncol* 2019;10:19–24. <https://doi.org/10.1016/j.phro.2019.04.004>.
- 25] Ahunbay EE, Peng C, Chen GP, Narayanan S, Yu C, Lawton C, et al. An on-line replanning scheme for interfractional variations. *Med Phys* 2008;35:3607–15. <https://doi.org/10.1118/1.2952443>.
- 26] Wendling M, McDermott LN, Mans A, Olaciregui-Ruiz I, Pecharrmán-Gallego R, Sonke J-J, et al. In aqua vivo EPID dosimetry. *Med Phys* 2012;39:367–77. <https://doi.org/10.1118/1.3665709>.
- 27] van der Bijl E, van Oers RFM, Olaciregui-Ruiz I, Mans A. Comparison of gamma- and DVH-based in vivo dosimetric plan evaluation for pelvic VMAT treatments. *Radiother Oncol* 2017;125:405–10. <https://doi.org/10.1016/j.radonc.2017.09.014>.
- 28] Olaciregui-Ruiz I, Torres-Xirau I, Teuwen J, van der Heide UA, Mans A. A Deep Learning-based correction to EPID dosimetry for attenuation and scatter in the Unity MR-Linac system. *Phys Med* 2020;71:124–31. <https://doi.org/10.1016/j.ejomp.2020.02.020>.
- 29] Mijnheer B, Jomehzadeh A, González P, Olaciregui-Ruiz I, Rozendaal R, Shokrani P, et al. Error detection during VMAT delivery using EPID-based 3D transit dosimetry. *Phys Med* 2018;54:137–45. <https://doi.org/10.1016/j.ejomp.2018.10.005>.
- 30] Roberts DA, Sandin C, Vesanan PT, Lee H, Hanson IM, Nill S, et al. Machine QA for the Elekta Unity system: A Report from the Elekta MR-linac consortium. *Med Phys* 2021;48:e67–85. <https://doi.org/10.1002/mp.14764>.
- 31] Olaciregui-Ruiz I, Rozendaal R, van Oers RFM, Mijnheer B, Mans A. Virtual patient 3D dose reconstruction using in air EPID measurements and a back-projection

- algorithm for IMRT and VMAT treatments. *Phys Med* 2017;37:49–57. <https://doi.org/10.1016/j.ejmp.2017.04.016>.
- [32] S.J. Hoogcarpsel S.E. Zijlema R.H.N. Tijssen L.G.W. Kerkmeijer I.M. Jürgenliemk-Schulz J.J.W. Lagendijk et al. Characterization of the first RF coil dedicated to 1.5 T MR guided radiotherapy *Phys Med Biol* 2018;63:025014. 10.1088/1361-6560/aaa303.
- [33] Rippke C, Schrenk O, Renkamp CK, Buchele C, Hörner-Rieber J, Debus J, et al. Quality assurance for on-table adaptive magnetic resonance guided radiation therapy: A software tool to complement secondary dose calculation and failure modes discovered in clinical routine. *J Appl Clin Med Phys* 2022;23:e13523.